Int. J. Electrochem. Sci., 17 **(2022)** Article Number: 221024, doi: 10.20964/2022.10.13

International Journal of
ELECTROCHEMICAL
SCIENCE
www.electrochemsci.org

Determination of water-soluble nitrate ions in PM2.5 particles using UiO-67 modified glassy carbon electrode

Ying Zhu[1,2,*] *and Zhiqiang Lv*[3]

[1] Henan Institute of Technology, Xinxiang, 453000, Henan, China
[2] Philippine Christian University International College, Manila, 1004, Philippines
[3] Xinxiang No. 1 Middle School, Xinxiang, 453000, Henan, China
[*]E-mail: zhu010056@163.com

Received: 9 June 2022 / *Accepted:* 23 July 2022 / *Published:* 10 September 2022

NO_3^- is the main component of PM2.5. NO_3^- will be converted into carcinogenic and teratogenic nitrite by microorganisms in the intestine after ingestion by human body. Therefore, it is particularly important to establish a rapid, sensitive, simple and accurate NO_3^- detection method. This work used UiO-67 directly as an electrode material to construct a UiO-67/glass carbon electrode (GCE) sensor. The work carefully investigated its electrochemical detection of NO_3^- in PM2.5. Its current response to NO_3^- was explored by cyclic voltammetry (CV), and a pair of reversible redox peaks was found. The work explored the effects of pH and interfering species on the sensing performance. The results showed that the differential pulse voltammetry (DPV) detected NO_3^- in the linear range of 6.67×10^{-6}~2.00×10^{-4} M at UiO-67/CCE with a detection limit of 2 μM. The sensor was successfully used for the detection of actual atmospheric PM 2.5 samples.

Keywords: Electrochemical detection; Metal-organic frameworks; Nitrate; PM 2.5; Air pollution

1. INTRODUCTION

With the accelerating industrialization and urbanization, energy consumption is rapidly increasing and the problem of air pollution is becoming serious. The essence of haze is fine particulate matter pollution (PM 2.5, aerodynamic diameter ≤ 2.5) [1–3]. It has been well established in many studies that PM25 pollution not only affects air quality, reduces atmospheric visibility, causes climate and ecosystem changes, but also poses important risks to human health, including increased mortality, reduced lung and immune function, lower fertility, and cardiovascular and respiratory diseases [4,5]. In addition, PM 2.5 pollution can also have many adverse effects on social and economic activities, such as delaying or canceling flights and closing highways. Secondary water-soluble inorganic ions such as SO_4^{2-}, NO_3^- and NH_4^+ (SNA) are important components of PM 2.5. They have strong hygroscopic and

indirect radiative forcing effects, and can directly affect the acidity of precipitation and the formation of cloud condensation nodules [6–8]. They are the main contributors to the atmospheric scattering extinction coefficient, which can greatly reduce the atmospheric visibility, and are also important components of the atmospheric regional complex pollution [9,10]. Therefore, studying the concentration level and pollution characteristics of SNA can help to analyze the source of PM 2.5 pollution and its impact on the environment.

SNA is mainly generated by gaseous precursors sulfur dioxide (SO_2), nitrogen oxides (NO_x), ammonia (NH_3) through homogeneous or non-homogeneous chemical reactions [11–13]. For example, SO_4^{2-} is mainly generated through gas-phase oxidation of SO_2, or by multiphase chemical reactions between SO_2 with H_2O_2 and O_3 in clouds. NO_3^- is mainly generated by homogeneous reactions of NO_x in the atmosphere first to form gaseous or liquid HNO_3, and then to react with NH_3 under NH_3-rich conditions [14–16]. Or it is generated by the non-homogeneous hydrolysis reaction of N_2O_5 on the surface of the particles under the conditions of NO_3 deficiency. In contrast, NH_4^+ is mainly generated by neutralization reactions between the only alkaline gas in the atmosphere (NH_3, mainly from emissions from agriculture, livestock, farming, etc.) and acidic H_2SO_4 and HNO_3 [17,18]. The formation of SNA depends largely on the nature of the present particulate matter, the level of occurrence of gaseous precursors, meteorological conditions, relative humidity, temperature, and atmospheric oxidants [19–22].

SNA is highly hygroscopic and can affect the chemical composition and optical characteristics of particulate matter [23–25]. It can affect cloud number by forming cloud condensation nuclei and cause indirect radiative forcing, thus indirectly affecting atmospheric visibility and global climate. Water-soluble ions are one of the most important factors affecting atmospheric visibility, with SNA contributing the most to visibility reduction. In addition, the acidity of PM 2.5 is determined by the content of water-soluble acidic and basic components [26]. The major acidic components are SO_4^{2-} and NO_3^-. The acidity of PM 2.5 has important effects on both the environment and human health. Acidic particulate can activate harmful components in the particulate matter and increase the risk to human health. Therefore, the study of SNA fraction in PM 2.5 is helpful to elucidate the main sources of PM 2.5 pollution, the formation mechanism and the impact on human health [27,28].

Along with the continuous improvement and refinement of analytical testing techniques, the detection methods for particulate matter PM 2.5 have been gradually improved. Scanning electron microscopy and transmission electron microscopy are used to analyze the structure of PM 2.5 and its constituent elements [29]. The determination of trace elements in PM 2.5 can be performed by plasma mass spectrometry, atomic absorption spectroscopy, plasma atomic emission spectroscopy, X-ray fluorescence spectroscopy, instrumental neutron activation analysis, etc. The determination of organic substances such as aromatic monsters adsorbed on PM 2.5 is usually performed by GC-MS or HPLC [30–33]. The chemically modified electrode is modified by chemically modifying the surface of the electrode with specific modifiers, so that the modified electrode has some specific properties and thus can make efficient and sensitive selection of the reaction. Therefore, the surface of the modified electrode provides a variety of properties that not only allow efficient separation and enrichment of the substance to be measured, but also combine the selectivity of the reaction as well as the sensitivity of the measurement [34–36]. Therefore, the chemically modified electrode is an ideal system that can

effectively combine separation, enrichment and measurement. Different types of modified electrodes can be produced by attaching different functional groups to the electrode surface according to different needs. There are various materials for electrode modification, and both metals and non-metals can be used as modifiers to modify the electrode surface. The sensitivity of most chemically modified electrodes is excellent, so that the modified electrodes can make accurate determination of trace or even ultra-trace substances [37–40]. Chemically modified electrodes have many advantages such as simple electrode preparation method, high sensitivity, good reproducibility and long service life, which make them widely used in the field of environmental monitoring.

Electrochemical methods are widely used in the field of PM 2.5 detection because of their low detection limits, low cost and simple operation. The main methods used for ion detection include anodic dissolution voltammetry, ion-selective electrodes, dissolution timing potentiometry, etc. In addition, the combination of electrochemical methods and biotechnology has led to the emergence of biosensors, which have become a popular research area in recent years [41–44]. The excellent performance of enzyme electrochemical sensors, immune-electrochemical sensors, and especially DNA electrochemical sensors in the detection of heavy metal ions has attracted the attention of scientists [45].

Currently, the commonly used methods for the detection of NO_3^- are polarimetry, fluorescence kinetic photometry, ultraviolet spectroscopy, and chromatography [46,47]. However, these methods are usually time-consuming and involve complex chemical reactions, or require large amounts of reagents, analytes and large and complex instruments [48]. Electrochemical methods are favored by researchers because they have many advantages such as fast detection speed, wide measurement range, and portability. Metal organic backbones (MOFs) are a class of porous crystalline materials assembled from metal ions or ion clusters bridged by organic ligands. It is of great interest in various fields such as catalyst adsorption, separation and drug delivery [49]. UiO series MOFs are three-dimensional porous materials containing one octahedral central cage and eight tetrahedral corner cages constructed from Zr and dicarboxylic acid ligands, such as: UiO-66, UiO-67, UiO-68, etc. Most of these MOFs have excellent stability, especially hydrothermal stability, and can be used as catalysts, sensor materials and adsorbents.

In this experiment, the UiO-67 material was synthesized by the solvent thermal method, and the material was modified with a CCE for the electrochemical detection of NO_3^- (Figure 1). The prepared UiO-67 materials were characterized by X-ray powder diffraction (XRD) and gas adsorption instrument for the physical phase, morphology, pore size and specific surface area, respectively. The properties of the electrodes were investigated by electrochemical impedance spectroscopy (EIS). It was found that the electron transport rate on the UiO-67 surface was better compared with that of the bare electrode. The linear range of 6.67×10^{-6}~2.00×10^{-4} M was determined by differential pulse voltammetry (DPV) with a detection limit of 2 μM under optimal experimental conditions.

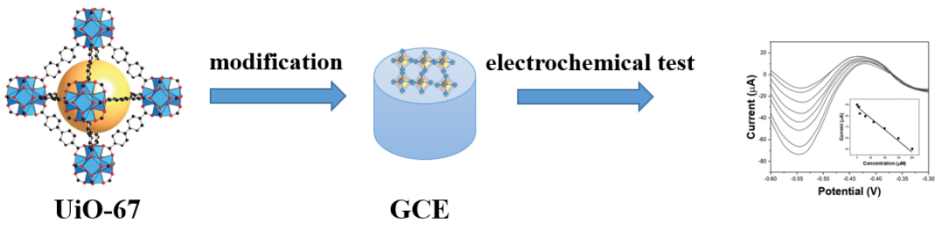

Figure 1. Schematic illustration of the fabrication of UiO-67/GCE sensors for determination of nitrate.

2. EXPERIMENTAL

2.1. Reagents and instruments

Zirconium tetrachloride (AR, alladdin Chemical Reagent Co., Ltd.), 4,4'-biphenyldicarboxylic acid (AR, alladdin Chemical Reagent Co., Ltd.), benzoic acid (AR, Shanghai Laize Fine Chemical Factory), acetone, sodium nitrate, ascorbic acid, magnesium sulfate, N,N'-dimethylformamide, calcium chloride, potassium chloride, copper chloride and glucose were all analytically pure and purchased from Sinopharm Chemical Reagent Co. Potassium chloride, copper chloride and glucose were all analytically pure and purchased from Sinopharm Chemical Reagent Co. The phosphate buffer solution (NaH_2PO_4-Na_2HPO_4) with different pH values was prepared by preparing 0.1 M NaH_2PO_4 and 0.1 M Na_2HPO_4 solutions in a certain volume ratio.

Powder X-ray diffraction (XRD) analysis was performed on a PAN alytical X'Pert3 powder diffractometer with CuKa radiation source. Thermogravimetric (TGA) curves were measured with a METTLER STDA 851° thermogravimetric analyzer (test temperature range: 30 ~ 600 °C under nitrogen atmosphere, 10 °C-min). Infrared spectroscopy (FT-IR) was performed with a Nicolet 5700 FT-IR spectrometer (KBr press, 4000-400 cm). Gas adsorption tests were performed on a Micromeritics ASAP 2020 analyzer. The electrochemical tests were performed on a CHI 660E (CHI Instruments, Shanghai, China).

2.2. Preparation of UiO-67

Weighed 0.120 g ZnCl and 0.125 g 4,4-biphenyldicarboxylic acid in a glass vial, and added 20 mL DMF solvent to dissolve them. Then 1.83 g of benzoic acid was added and sonicated for 5 min. Finally, the cap was tightened and placed in an oven at 100 ℃ for 2 d. The product was cooled to room temperature, centrifuged, and UiO-67 product was obtained at the bottom of the centrifuge tube. The activation of UiO-67 was carried out by solvent exchange method. The UiO-67 powder was washed three times with DMF and acetone in order to remove the unreacted ligands and metal ions, and finally the product was dried at 80 ℃.

2.3. Electrochemical test

The GCE (3 mm) was polished with Al_2O_3 grinding powder of 1.0, 0.3 and 0.05 μm particle size on chamois in turn. After each polishing, the electrodes were ultrasonicated with anhydrous ethanol and water for 2 min to remove impurities on the electrode surface and dried under an infrared lamp. After weighing 4 mg of UiO-67 in 1 mL of anhydrous ethanol, the dispersion was dispersed well with ultrasound and 10 uL of the dispersion was applied to the polished GCE surface, and then dried under an infrared lamp. Finally, 5 uL of 0.5% Nafion was added dropwise to the electrode surface to obtain UiO-67/GCE. The electrochemical experiments were performed using the conventional three-electrode system, in which the GCE was the working electrode, the saturated Ag/AgCl electrode was the reference electrode and the platinum wire was the auxiliary electrode.

3. RESULTS AND DISCUSSION

The XRD pattern of UiO-67 is shown in Figure 2A. It can be seen that the XRD peaks of the synthesized UiO-67 are almost identical to the simulated ones [50], which indicates that UiO-67 has been successfully synthesized.

Figure 2B shows the TGA curves of the activated UiO-67. From Figure 2B, it can be seen that the prepared UiO-67 has three main weight loss plateaus. The first weight loss platform has a temperature variation range of 30-60 ℃, which is generated by the weight loss of residual acetone in the material. The second weight-loss plateau is from 100 to 400 °C, which is mainly due to the removal of solvent from the material. The third weight loss plateau has a temperature variation range of 400~600 °C, which is due to the weight loss caused by the collapse of the metal-organic structure [51,52]. The above results indicate that UiO-67 has excellent thermal stability [53].

The results of FTIR analysis of UiO-67 material are shown in Figure 2C. As can be seen from the spectrum: 3430 cm^{-1} corresponds to the -OH stretching vibration peak, indicating the presence of -OH in the material [54]. The characteristic absorption peaks at 1592 and 1421 cm^{-1} correspond to the carboxylate ion C-O and benzene ring, respectively.

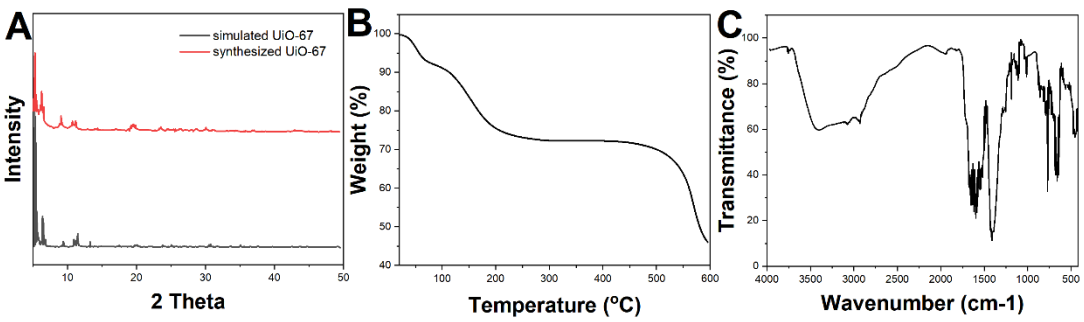

Figure 2. (A) XRD pattern, (B) TGA curve and (C) FTIR spectrum of UiO-67.

To evaluate the effect of the pore properties of UiO-67, a series of N adsorption isotherms were collected at -196 ℃, and the results are shown in Figure 3A. The isothermal adsorption curve of UiO-67 is type I isotherm, which indicates that the sample is a microporous material [55]. The corresponding pore size distribution curves are shown in Figure 3B, which indicates that the pore size distribution is mainly around 1 nm.

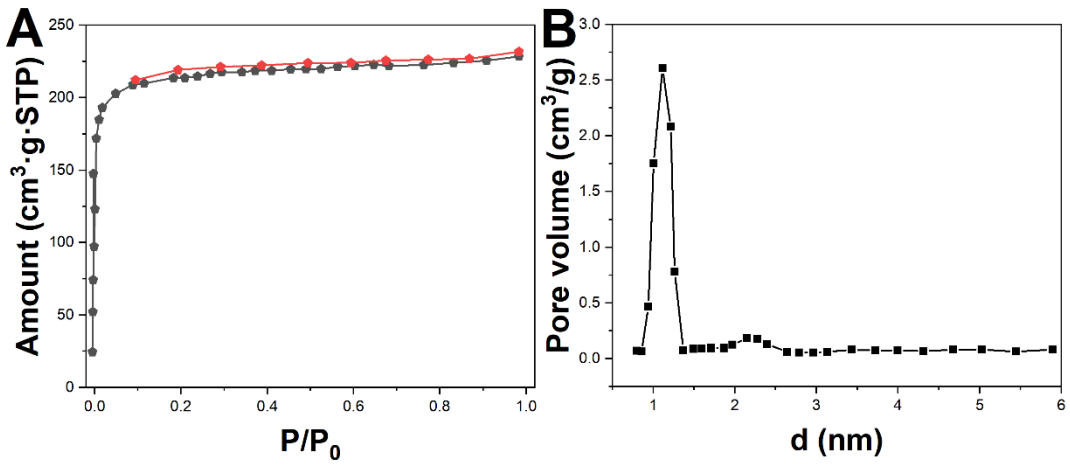

Figure 3. (A) 77 K N2 sorption isotherms and (B) pore-size distribution of UiO-67 calculated by using a slit NLDFT model.

Figure 4A shows the EIS plots of GCE and UiO-67/GCE. Figure 4B shows the Bode plot EIS spectra of the same electrodes as shown in Figure 4A with the phase shifts and absolute values of the impedance plotted against the tested frequencies. The resistance value of GCE is obviously much larger than that of the porous copper modified electrode, indicating that the bare electrode was successfully modified to UiO-67, thus contributing to the electron transfer [56].

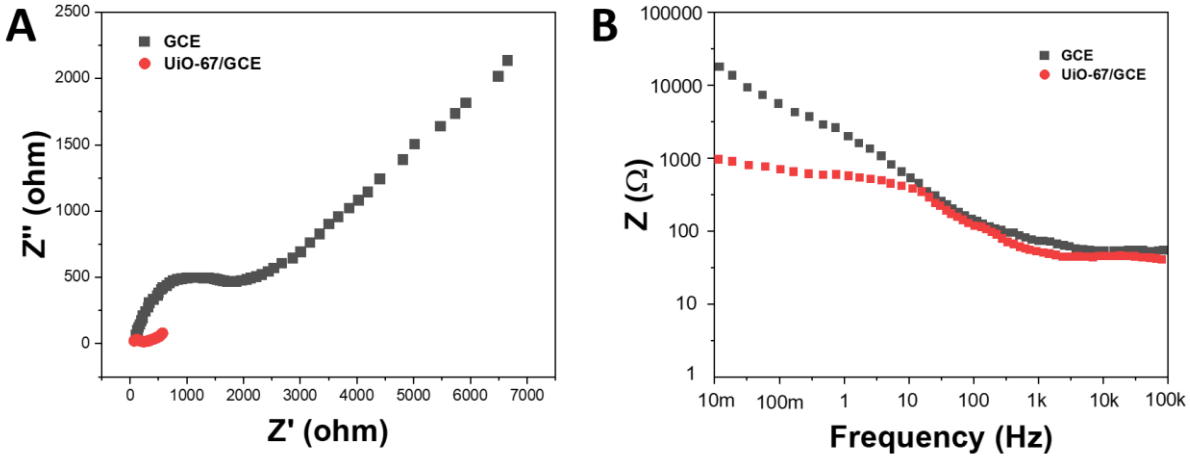

Figure 4. (A) EIS plots and (B) Bode plots of GCE and UiO-67/GCE in 5 mM $Fe(CN)_6^{3-}/Fe(CN)_6^{4-}$ +0.01 M KCl.

The CV curves of UiO-67/GCE were compared with those of GCE in a NO_3^- containing electrolyte (0.1M Na_2SO_4, pH=3.0). As can be seen from Figure 5A, the curve of GCE in the test solution showed no reduction peak near -0.55 V, while UiO-67/GCE had a clear reduction peak at -0.55 V. This

indicates that the modification of a layer of UiO-67 on the electrode surface is more sensitive to the response of nitrate ions [57,58].

We tested the electrochemical properties of UiO-67/GCE in different electrolytes. We tested 0.1 M solutions of Na_2SO_4, Na_2CO_3, $NaHCO_3$, and $(NH_4)_2SO_4$ containing equal concentrations of NO_3^-, respectively. As can be seen from Figure 5B, the sensitivity of the determination was better with the choice of 0.1 M Na_2SO_4 as the supporting electrolyte.

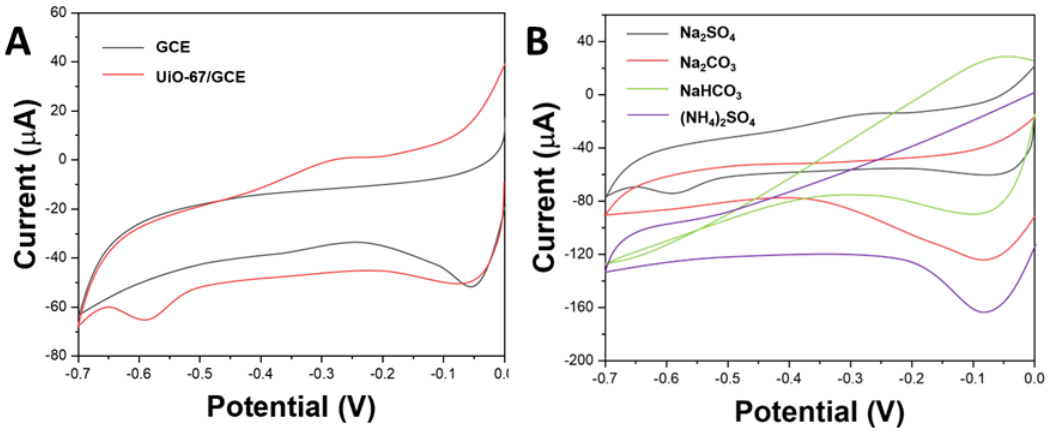

Figure 5. (A) Cyclic voltammetry of GCE and UiO-67/GCE in 1.00×10^{-5} M NO_3^- of 0.1 M Na_2SO_4（pH=3.0) base solution. The scan rate is 100 mV/s. (B) The influence of the electrolyte for the determination of 1.00×10^{-5} M NO_3^-. The scan rate is 100 mV/s.

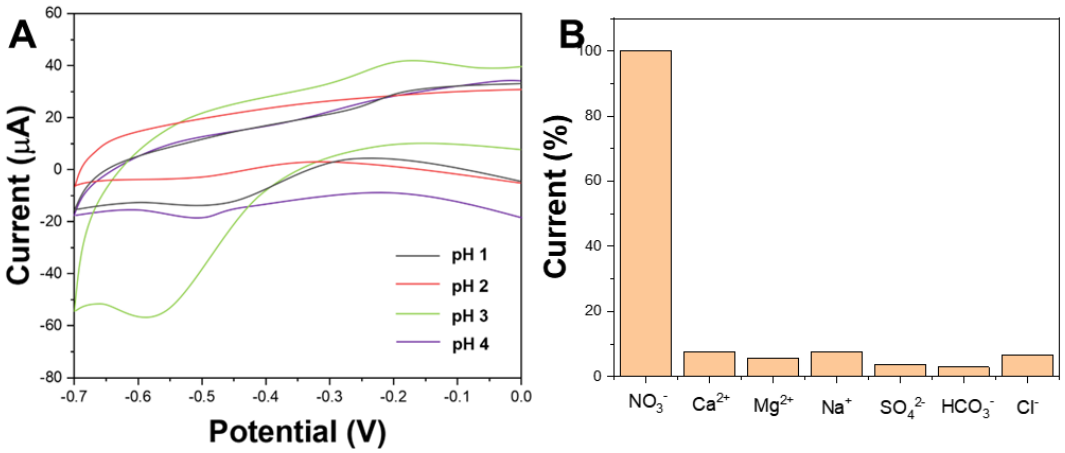

Figure 6. (A) The influence of the pH of electrolyte for the determination of 1.00×10^{-5} M NO_3^-. The scan rate is 100 mV/s. (B) The interference study of the UiO-67/GCE towards 1.00×10^{-5} M NO_3^- at pH 3.0 Na_2SO_4.

The variation of the voltammetric response of UiO-67/GCE to NO_3^- in Na_2SO_4 with pH ranging from 0.0 to 4.0 is given in Figure 6A. From the figure, it can be seen that the difference in pH of the electrolyte affects the voltammetric response and has a greater effect on the catalytic reduction of NO_3^-

[59]. The current response showed maximum when the pH was 3.0, so the electrolyte with pH 3.0 was chosen.

Figure 6B shows the interference of UiO-67/GCE with other common ions (SO_4^{2-}, Cl^-, HCO_3^-, Na^+, Ca^{2+}, Mg^{2+}) in PM 2.5 for the determination of NO_3^-. The results showed that none of these ions interfered significantly with the determination.

Figure 7 shows the peak current of the electrode in Na_2SO_4 solution at pH=3 versus 6.67×10^{-6} to 2.00×10^{-4} M nitrate concentration. It can be seen from the figure that the peak current has a good linear relationship with the nitrate concentration with a linear correlation coefficient of 0.994. The detection limit of the determination can be calculated to be 2.00×10^{-6} M. Table 1 shows the comparison of the proposed electrochemical sensor with previous reports.

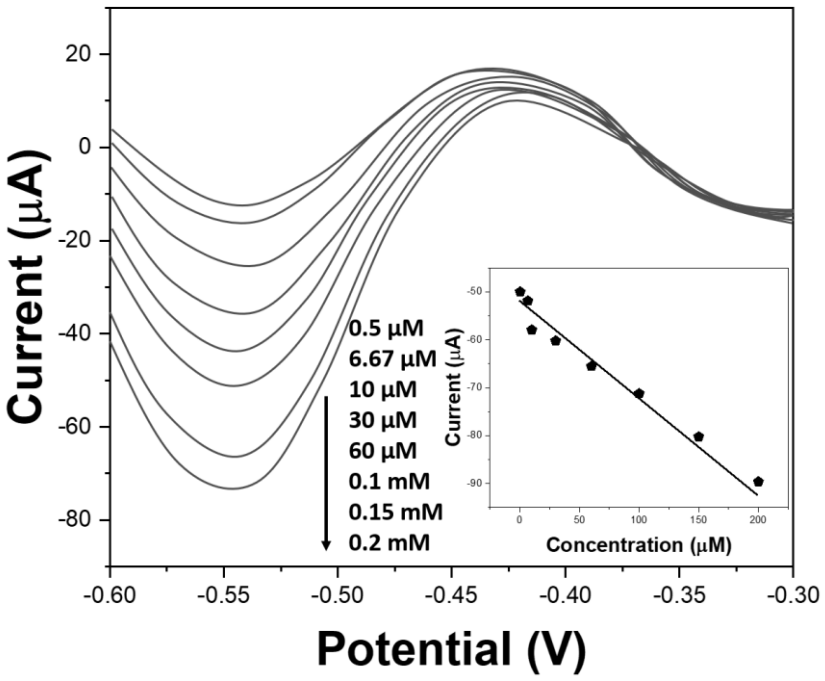

Figure 7. DPV of different concentrations of NO_3^- on the UiO-67/GCE in 0.1 M Na_2SO_4(pH=3.0). Inset was the linearity between the concentration of NO_3^- and peak current.

Table 1. Comparison of the proposed UiO-67/GCE with previous reported electrochemical sensors toward NO_3^- detection.

Sensor	Linear detection range	Limit of detection	Reference
Au/GO-CS/GCE	0.9–18.9 μM	0.3 μM	[60]
Pt-GO-PB	-	6.6 μM	[61]
Ag-RGO/GCE	0.1–120 μM	0.012 μM	[62]
CuO/H-C3N4/RGO	0.2–110 μM	0.016 μM	[63]
UiO-67/GCE	6.67×10^{-6} to 2.00×10^{-4} M	2.00×10^{-6} M	This work

Table 2. The results of electrochemical test and ion chromatography test for detecting the NO_3^- in PM 2.5 particle.

Sample	UiO-67/GCE (10^{-5} M)	IC (10^{-5} M)	SD (%)	In air (μg/m^3)
1	1.58	1.56	1.31	0.19
2	1.80	1.88	0.95	0.11
3	2.04	2.07	1.08	0.08

We obtained the actual PM 2.5 samples from Xinxiang City Environmental Monitoring Station, measured with UiO-67/GCE and compared the test results with those of ion chromatography. The actual paper strip samples were soaked in Na_2SO_4 solution at pH 3.0 for 48 h. Each sample was divided into two parts, one part of the sample was tested using the UiO-67/GCE developed in this paper and the other part was determined using ion chromatography [64]. Table 1 shows the test results of NO_3^--content in the samples measured by electrochemical and ion chromatography methods. From Table 2, it can be seen that the relative deviations between the test results of UiO-67/GCE and the test values of ion chromatography method ranged from 0.95 to 1.31%.

4. CONCLUSION

In this work, we synthesized UiO-67 by a solvent method and constructed the material as an electrochemical sensor that can be used to detect NO_3^-. Under the optimal conditions, the linear range of NO_3^- response on UiO-67/CCE was 6.67×10^{-6}~2.00×10^{-4} M, and the detection limit was 2 μM (S/N=3). The sensor was used for the detection of real air PM2.5 samples with relative deviations between 0.95 and 1.31%.

References

1. M. Badura, I. Sówka, P. Szymański, P. Batog, *Sci. Total Environ.*, 722 (2020) 137867.
2. C. -H. Weng, G. Pillai, S. -S. Li, *IEEE Sens. J.*, 20 (2020) 14722–14731.
3. R. Cao, B. Li, Z. Wang, Z.-R. Peng, S. Tao, S. Lou, *Environ. Pollut.*, 264 (2020) 114549.
4. D. Fahimi, O. Mahdavipour, J. Sabino, R.M. White, I. Paprotny, *Sens. Actuators Phys.*, 299 (2019) 111569.
5. B. Feenstra, V. Papapostolou, S. Hasheminassab, H. Zhang, B.D. Boghossian, D. Cocker, A. Polidori, *Atmos. Environ.*, 216 (2019) 116946.
6. C.-H. Lee, Y.-B. Wang, H.-L. Yu, *Environ. Int.*, 130 (2019) 104838.
7. Y. Li, S. Yuan, S. Fan, Y. Song, Z. Wang, Z. Yu, Q. Yu, Y. Liu, *Curr. Pollut. Rep.*, 7 (2021) 72–87.
8. Y. Lu, G. Giuliano, R. Habre, *Environ. Res.*, 195 (2021) 110653.

9. S.-C.C. Lung, W.-C.V. Wang, T.-Y.J. Wen, C.-H. Liu, S.-C. Hu, *Sci. Total Environ.*, 716 (2020) 137145.
10. X. Qiao, Q. Zhang, D. Wang, J. Hao, J. Jiang, *Sci. Total Environ.*, 779 (2021) 146381.
11. K. Ali, P. Acharja, D.K. Trivedi, R. Kulkarni, P. Pithani, P.D. Safai, D.M. Chate, S. Ghude, R.K. Jenamani, M. Rajeevan, *Sci. Total Environ.*, 662 (2019) 687–696.
12. X.-C. Chen, T.J. Ward, J.-J. Cao, S.-C. Lee, N.-C. Lau, S.HL. Yim, K.-F. Ho, *Atmos. Environ.*, 218 (2019) 116999.
13. M.-B. Park, T.-J. Lee, E.-S. Lee, D.-S. Kim, *Atmospheric Pollut. Res.*, 10 (2019) 1042–1059.
14. Y. Ren, J. Wei, Z. Wu, Y. Ji, F. Bi, R. Gao, X. Wang, G. Wang, H. Li, *Atmospheric Res.*, 251 (2021) 105412.
15. W. Sun, D. Wang, L. Yao, H. Fu, Q. Fu, H. Wang, Q. Li, L. Wang, X. Yang, A. Xian, G. Wang, H. Xiao, J. Chen, *Environ. Pollut.*, 254 (2019) 112864.
16. E. Tutsak, M. Koçak, *Sci. Total Environ.*, 672 (2019) 212–226.
17. X. Wang, W. Wei, S. Cheng, S. Yao, H. Zhang, C. Zhang, *Atmospheric Pollut. Res.*, 10 (2019) 1976–1984.
18. L. Yang, Y. Shang, M.P. Hannigan, R. Zhu, Q. Wang, C. Qin, M. Xie, *Atmos. Environ.*, 246 (2021) 118066.
19. S. Yu, W. Liu, Y. Xu, K. Yi, M. Zhou, S. Tao, W. Liu, *Sci. Total Environ.*, 650 (2019) 277–287.
20. J. Zhang, H. Cheng, D. Wang, Y. Zhu, C. Yang, Y. Shen, J. Yu, Y. Li, S. Xu, X. Song, Y. Zhou, J. Chen, L. Fan, J. Jiang, C. Wang, K. Hao, *Environ. Pollut.*, 280 (2021) 116951.
21. Q. Zhang, G. Geng, *Sci. China Earth Sci.*, 62 (2019) 1845–1846.
22. W. Zhang, B. Liu, Y. Zhang, Y. Li, X. Sun, Y. Gu, C. Dai, N. Li, C. Song, Q. Dai, Y. Han, Y. Feng, *Atmos. Environ.*, 222 (2020) 117157.
23. Q.-L. Cai, X.-R. Dai, J.-R. Li, L. Tong, Y. Hui, M.-Y. Cao, M. Li, H. Xiao, *Sci. Total Environ.*, 709 (2020) 136146.
24. K. Dimitriou, N. Mihalopoulos, S.R. Leeson, M.M. Twigg, *Chemosphere*, 274 (2021) 129979.
25. Y. Ding, M. Zhang, X. Qian, C. Li, S. Chen, W. Wang, *J. Clean. Prod.*, 211 (2019) 1480–1490.
26. H. Hassan, M.T. Latif, L. Juneng, N. Amil, M.F. Khan, Y. Fujii, A.A. Jamhari, H.H.A. Hamid, T. Banerjee, *Urban Clim.*, 39 (2021) 100953.
27. K. Juda-Rezler, M. Reizer, K. Maciejewska, B. Błaszczak, K. Klejnowski, *Sci. Total Environ.*, 713 (2020) 136729.
28. F. Liu, Q. Tan, X. Jiang, F. Yang, W. Jiang, *J. Environ. Sci.*, 86 (2019) 15–23.
29. P. Masselot, F. Sera, R. Schneider, H. Kan, É. Lavigne, M. Stafoggia, A. Tobias, H. Chen, R.T. Burnett, J. Schwartz, A. Zanobetti, M.L. Bell, B.-Y. Chen, Y.-L.L. Guo, M.S. Ragettli, A.M. Vicedo-Cabrera, C. Åström, B. Forsberg, C. Íñiguez, R.M. Garland, N. Scovronick, J. Madureira, B. Nunes, C. De la Cruz Valencia, M. Hurtado Diaz, Y. Honda, M. Hashizume, C.F.C. Ng, E. Samoli, K. Katsouyanni, A. Schneider, S. Breitner, N.R.I. Ryti, J.J.K. Jaakkola, M. Maasikmets, H. Orru, Y. Guo, N. Valdés Ortega, P. Matus Correa, S. Tong, A. Gasparrini, *Epidemiology*, 33 (2021) 167–175.
30. S.-C. Son, G.-H. Yu, S. Park, S. Lee, *Atmospheric Pollut. Res.*, 12 (2021) 101199.
31. Z. Sun, F. Duan, K. He, J. Du, L. Zhu, *Sci. Total Environ.*, 647 (2019) 204–209.
32. M. in ’t Veld, A. Alastuey, M. Pandolfi, F. Amato, N. Pérez, C. Reche, M. Via, M.C. Minguillón, M. Escudero, X. Querol, *Sci. Total Environ.*, 795 (2021) 148728.
33. J. Williams, L. Petrik, J. Wichmann, *Air Qual. Atmosphere Health*, 14 (2021) 431–442.
34. W. Xing, L. Yang, H. Zhang, X. Zhang, Y. Wang, P. Bai, L. Zhang, K. Hayakawa, S. Nagao, N. Tang, *Atmospheric Pollut. Res.*, 12 (2021) 101233.
35. Q. Xu, S. Wang, J. Jiang, N. Bhattarai, X. Li, X. Chang, X. Qiu, M. Zheng, Y. Hua, J. Hao, *Sci. Total Environ.*, 689 (2019) 1293–1303.
36. C. Yan, S. Ma, Q. He, X. Ding, Y. Cheng, M. Cui, X. Wang, M. Zheng, *Atmos. Environ.*, 246 (2021) 118069.

37. W. Zhang, X. Peng, X. Bi, Y. Cheng, D. Liang, J. Wu, Y. Tian, Y. Zhang, Y. Feng, *Atmos. Environ.*, 244 (2021) 117942.
38. H. Karimi-Maleh, M. Alizadeh, Y. Orooji, F. Karimi, M. Baghayeri, J. Rouhi, S. Tajik, H. Beitollahi, S. Agarwal, V.K. Gupta, S. Rajendran, S. Rostamnia, L. Fu, F. Saberi-Movahed, S. Malekmohammadi, *Ind. Eng. Chem. Res.*, 60 (2021) 816–823.
39. H. Karimi-Maleh, C. Karaman, O. Karaman, F. Karimi, Y. Vasseghian, L. Fu, M. Baghayeri, J. Rouhi, P. Senthil Kumar, P.-L. Show, S. Rajendran, A.L. Sanati, A. Mirabi, *J. Nanostructure Chem.*, 12 (2022) 429–439.
40. H. Karimi-Maleh, H. Beitollahi, P.S. Kumar, S. Tajik, P.M. Jahani, F. Karimi, C. Karaman, Y. Vasseghian, M. Baghayeri, J. Rouhi, *Food Chem. Toxicol.* (2022) 112961.
41. W. Guo, Z. Zhang, N. Zheng, L. Luo, H. Xiao, H. Xiao, *Atmospheric Res.*, 234 (2020) 104687.
42. H. Karimi-Maleh, Y. Orooji, F. Karimi, M. Alizadeh, M. Baghayeri, J. Rouhi, S. Tajik, H. Beitollahi, S. Agarwal, V.K. Gupta, *Biosens. Bioelectron.*, 184 (2021) 113252.
43. H. Karimi-Maleh, A. Khataee, F. Karimi, M. Baghayeri, L. Fu, J. Rouhi, C. Karaman, O. Karaman, R. Boukherroub, *Chemosphere*, 291 (2021) 132928.
44. H. Karimi-Maleh, F. Karimi, L. Fu, A.L. Sanati, M. Alizadeh, C. Karaman, Y. Orooji, *J. Hazard. Mater.*, 423 (2022) 127058.
45. T. Liu, B. Hu, X. Xu, Y. Hong, Y. Zhang, X. Wu, L. Xu, M. Li, Y. Chen, X. Chen, J. Chen, *Atmos. Environ.*, 237 (2020) 117710.
46. M.R. Awual, M.M. Hasan, A. Islam, M.M. Rahman, A.M. Asiri, M.A. Khaleque, M.C. Sheikh, *J. Clean. Prod.*, 228 (2019) 778–785.
47. H. Chen, T. Yang, F. Liu, W. Li, *Sens. Actuators B Chem.*, 286 (2019) 401–407.
48. C.-Y. Hou, L.-M. Fu, W.-J. Ju, P.-Y. Wu, *Chem. Eng. J.*, 398 (2020) 125573.
49. X. Li, J. Ping, Y. Ying, *TrAC Trends Anal. Chem.*, 113 (2019) 1–12.
50. C.-S. Cao, J. Wang, X. Yu, Y. Zhang, L. Zhu, *Appl. Catal. B Environ.*, 277 (2020) 119222.
51. P. Chen, S. Liu, Z. Bai, Y. Liu, *Microporous Mesoporous Mater.*, 305 (2020) 110369.
52. G. Dai, Z. Li, F. Luo, S. Ai, B. Chen, Q. Wang, *Microchim. Acta*, 186 (2019) 620.
53. C.-X. Lü, G.-P. Zhan, K. Chen, Z.-K. Liu, C.-D. Wu, *Appl. Catal. B Environ.*, 279 (2020) 119350.
54. M. Lu, Y. Deng, Y. Li, T. Li, J. Xu, S.-W. Chen, J. Wang, *Anal. Chim. Acta*, 1110 (2020) 35–43.
55. S. Sun, P. Liao, L. Zeng, L. He, J. Zhang, *RSC Adv.*, 10 (2020) 14778–14784.
56. S. Zhang, Y. Wang, Z. Cao, J. Xu, J. Hu, Y. Huang, C. Cui, H. Liu, H. Wang, *Chem. Eng. J.*, 381 (2020) 122771.
57. R. Abazari, L. Esrafili, A. Morsali, Y. Wu, J. Gao, *Appl. Catal. B Environ.*, 283 (2021) 119582.
58. Y. An, Y. Liu, H. Bian, Z. Wang, P. Wang, Z. Zheng, Y. Dai, M.-H. Whangbo, B. Huang, *Sci. Bull.*, 64 (2019) 1502–1509.
59. A.H. Vahabi, F. Norouzi, E. Sheibani, M. Rahimi-Nasrabadi, *Coord. Chem. Rev.*, 445 (2021) 214050.
60. R. Mo, X. Wang, Q. Yuan, X. Yan, T. Su, Y. Feng, L. Lv, C. Zhou, P. Hong, S. Sun, *Sensors*, 18 (2018) 1986.
61. A.S. Adekunle, S. Lebogang, P.L. Gwala, T.P. Tsele, L.O. Olasunkanmi, F.O. Esther, D. Boikanyo, N. Mphuthi, J.A. Oyekunle, A.O. Ogunfowokan, *RSC Adv.*, 5 (2015) 27759–27774.
62. R. Ahmad, T. Mahmoudi, M.-S. Ahn, J.-Y. Yoo, Y.-B. Hahn, *J. Colloid Interface Sci.*, 516 (2018) 67–75.
63. Y. Li, C. Cheng, Y. Yang, X. Dun, J. Gao, X.-J. Jin, *J. Alloys Compd.*, 798 (2019) 764–772.
64. L. Yang, Y. Liu, L. Chen, L. Guo, Y. Lei, L. Wang, *Spectrochim. Acta. A. Mol. Biomol. Spectrosc.*, 261 (2021) 120068.